Monte Carlo calculations of k_Q, the beam quality conversion factor

B. R. Muir[a)] and D. W. O. Rogers[b)]
Ottawa Carleton Institute for Physics, Carleton University Campus, 1125 Colonel By Drive, Ottawa, Ontario K1S 5B6, Canada

(Received 17 May 2010; revised 9 August 2010; accepted for publication 7 September 2010; published 27 October 2010)

Purpose: To use EGSnrc Monte Carlo simulations to directly calculate beam quality conversion factors, k_Q, for 32 cylindrical ionization chambers over a range of beam qualities and to quantify the effect of systematic uncertainties on Monte Carlo calculations of k_Q. These factors are required to use the TG-51 or TRS-398 clinical dosimetry protocols for calibrating external radiotherapy beams.
Methods: Ionization chambers are modeled either from blueprints or manufacturers' user's manuals. The dose-to-air in the chamber is calculated using the EGSnrc user-code egs_chamber using 11 different tabulated clinical photon spectra for the incident beams. The dose to a small volume of water is also calculated in the absence of the chamber at the midpoint of the chamber on its central axis. Using a simple equation, k_Q is calculated from these quantities under the assumption that W/e is constant with energy and compared to TG-51 protocol and measured values.
Results: Polynomial fits to the Monte Carlo calculated k_Q factors as a function of beam quality expressed as $\%dd(10)_x$ and TPR_{10}^{20} are given for each ionization chamber. Differences are explained between Monte Carlo calculated values and values from the TG-51 protocol or calculated using the computer program used for TG-51 calculations. Systematic uncertainties in calculated k_Q values are analyzed and amount to a maximum of one standard deviation uncertainty of 0.99% if one assumes that photon cross-section uncertainties are uncorrelated and 0.63% if they are assumed correlated. The largest components of the uncertainty are the constancy of W/e and the uncertainty in the cross-section for photons in water.
Conclusions: It is now possible to calculate k_Q directly using Monte Carlo simulations. Monte Carlo calculations for most ionization chambers give results which are comparable to TG-51 values. Discrepancies can be explained using individual Monte Carlo calculations of various correction factors which are more accurate than previously used values. For small ionization chambers with central electrodes composed of high-Z materials, the effect of the central electrode is much larger than that for the aluminum electrodes in Farmer chambers. © *2010 American Association of Physicists in Medicine*. [DOI: 10.1118/1.3495537]

Key words: beam quality conversion factor, k_Q, EGSnrc, dosimetry protocols, photon beams, Monte Carlo

I. INTRODUCTION

Clinical radiation sources are calibrated under reference conditions by following protocols based on ion chambers calibrated using absorbed dose-to-water standards.[1,2] Ionization chambers are calibrated by primary standards laboratories or accredited dosimetry calibration laboratories in terms of the absorbed dose-to-water in a cobalt-60 beam. In photon beams, the use of the beam quality conversion factor, k_Q, is required along with the absorbed dose-to-water calibration coefficient in a cobalt-60 beam, $N_{D,w}^{^{60}\mathrm{Co}}$, to convert the corrected reading, M, of the ion chamber in an arbitrary beam of quality Q to the absorbed dose-to-water, D_w, using

$$D_w^Q = MN_{D,w}^Q = Mk_Q N_{D,w}^{^{60}\mathrm{Co}}. \tag{1}$$

The k_Q factor varies with beam quality and ionization chamber geometry and materials. The protocols in use provide tables of the beam quality conversion factor for some of the commercially available ion chambers. However, many chambers now exist for which values are not available, including small chambers used to improve spatial resolution for other applications.

In the dosimetry protocols, the approach to calculating k_Q was based on taking the ratio at two beam qualities of the product of several correction factors and the Spencer–Attix stopping-power ratio between water and air, $(\bar{L}/\rho)_{\mathrm{air}}^{\mathrm{water}}$, viz.,

$$k_Q = \left[\left(\frac{\bar{L}}{\rho}\right)_{\mathrm{air}}^{\mathrm{water}} P_{\mathrm{cel}} P_{\mathrm{repl}} P_{\mathrm{wall}}\right]_{^{60}\mathrm{Co}}^{Q}, \tag{2}$$

where P_{cel} corrects for the presence of a central electrode, P_{wall} corrects for the wall of the chamber being made of a different material than water, and P_{repl} corrects for changes in the electron spectrum due to the introduction of a cavity. The notation outside the bracket indicates that the terms inside the brackets are evaluated at a beam quality Q and in a cobalt-60 beam; the ratio of the two is calculated.

Previous publications have shown that some of the individual correction factors on which k_Q is based differ from Monte Carlo calculated values.[3–5] Consequently, there is

considerable motivation to verify previous k_Q calculations and to provide calculations for those chambers not available in the protocols. The goal of this work is to calculate the beam quality conversion factor directly using Monte Carlo simulations of a ratio at two beam qualities, namely,

$$k_Q = \left(\frac{D_w}{D_{ch}}\right)^{Q}_{^{60}\mathrm{Co}}, \tag{3}$$

relating the absorbed dose-to-water in the absence of the chamber at the location of the point of measurement, D_w, to the absorbed dose-to-air in the ion chamber averaged over the cavity volume, D_{ch}. The assumption is made that the average energy lost per Coulomb of charge released by electrons in air, W/e, is independent of beam quality. Previous studies have used the same approach to calculate the beam quality conversion factor for a subset of cylindrical ionization chambers.[4,6,7] These studies provide comparisons with the values calculated in this work. In addition, a comparison will be made between the results from this work and those from experimental investigations of k_Q.[8–10]

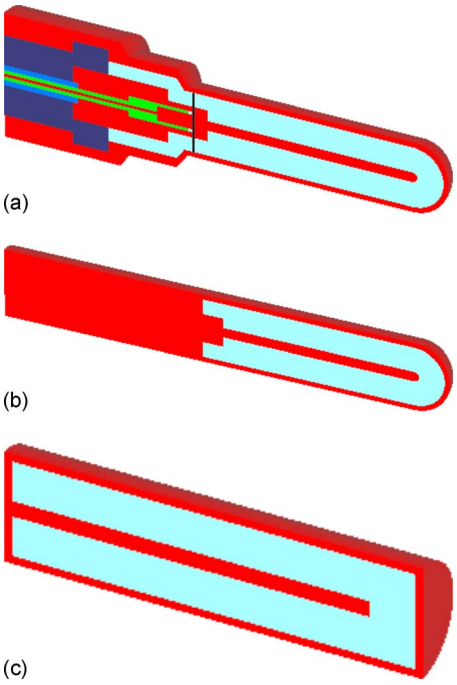

FIG. 1. Three models of the Exradin A12 ionization chamber (scales differ). (a) Blueprint model; the solid line shows where the active cavity begins; (b) user manual, with a spherical top and a 2 cm long stem; (c) user manual, purely cylindrical geometry.

II. METHODS

II.A. Calculation of absorbed dose

Simulations are performed using the EGSnrc[11,12] Monte Carlo code system with the egs_chamber user-code of Wulff *et al.*[13] Geometries are modeled with the egs++ geometry package.[14] Variance reduction techniques such as photon cross-section enhancement and correlated sampling are employed to save CPU time. Calculations of each of the four terms in Eq. (3) are performed. The default Monte Carlo transport parameters are used with the exception of the use of NIST bremsstrahlung cross-sections and XCOM photon cross-sections. The cutoff energies and production thresholds are set to 521 keV for electrons and 10 keV for photons. Simulations were performed with cutoff energies and production thresholds set to 512 and 1 keV for electrons and photons, respectively, for a chamber with a small volume. The effect of using the reduced cutoff energies and production thresholds for k_Q calculations was found to be negligible in the energy range of interest.

All quantities are calculated in a $30\times30\times30$ cm^3 water phantom at the point of measurement. In cobalt-60 beams, the point of measurement is on the central axis of the beam which is centered in the phantom and is at a depth of 5 cm. In all other beams, the point of measurement is at 10 cm depth. Cobalt-60 calculations are performed at 5 cm depth because this coincides with the calibration depth at calibration laboratories. Simulations for cobalt-60 were also performed at a depth of 10 cm and the difference in k_Q values was found to be less than 0.1%. The absorbed dose-to-water is calculated for a disk of water with a thickness of 0.025 cm and a radius of 1 cm centered on the point of measurement.

Thirty-two ionization chambers are modeled according to specifications from manufacturers' user's manuals or catalogs. The IBA CC01 is modeled using technical drawings from IBA. The Exradin ionization chambers are modeled using blueprint specifications and some results for k_Q are compared to the results for simplified models. Figure 1 shows the Exradin A12 chamber modeled from the blueprint along with two simplified models. The comparison between simulations performed using the three models yields a spread in k_Q values of less than 0.2% with a relative statistical uncertainty on the values of 0.1%. Similarly, Tantot and Seuntjens[7] state that the dose-to-air in the Exradin A12 chamber did not change significantly when all stem materials are changed to C552. For some chambers, a comparison of k_Q factors calculated with detailed and simplified models yields a larger difference. The use of simplified chamber models for a cavity dose calculation reduces the computing time by a factor of 2 compared to the same calculation with a full chamber model. However, all calculated k_Q factors provided in this work use detailed models from blueprint specifications where available. The PTW Farmer-type chambers are modeled using specifications from the PTW Product Catalog for the materials and dimensions. The geometry is based on the original chamber design by Aird and Farmer.[15] The NE2571 model is based on the model used by La Russa *et al.*[16] The PTW 31010 chamber is based on the model given by Wulff *et al.*[4] The ionization chambers that are used are given in Table I, along with the wall and electrode materials and chamber dimensions. The Exradin blueprint dimensions are proprietary so the specifications from the user's manual are given, although the simulations of Exradin ion chambers use blueprint models. For all chambers that are not inherently waterproof a 1 mm polymethylmethacrylate

TABLE I. The specifications of the ionization chamber models used. The materials are air equivalent plastic (C552), tissue equivalent plastic (A150), silver-plated copper-covered steel (SPC), PMMA, graphite (Gr), aluminum (Al), and polyoxymethylene (POM). The chambers are loosely divided into nine groups designated by the letters a–i with similar characteristics as described in the text. Each chamber's group is given here. The cavity length is the maximum length of the cavity. Chambers that are not waterproof are modeled with a 1 mm thick PMMA sleeve.

	Wall		Electrode			Active cavity		
Chamber [group, V(cm^3)]	Material	Thickness (mm)	Material	Radius (mm)	Length (mm)	Radius (mm)	Length (mm)	Waterproof
			Exradin					
A12 (a, 0.65)	C552	0.5	C552	0.5	21.6	3.05	24.8	Y
A19 (a, 0.62)	C552	0.5	C552	0.5	21.6	3.05	25.0	Y
A2 (a, 0.54)	C552	1.0	C552	0.5	8.4	4.7	12.0	Y
T2 (b, 0.54)	A150	1.0	A150	0.5	8.4	4.7	12.0	Y
A12S (a, 0.25)	C552	0.5	C552	0.5	7.4	3.05	10.6	Y
A18 (a, 0.125)	C552	1.0	C552	0.5	5.9	2.45	8.3	Y
A1 (a, 0.057)	C552	1.0	C552	0.5	4.4	2.0	6.0	Y
T1 (b, 0.057)	A150	1.0	A150	0.5	4.4	2.0	6.0	Y
A1SL (a, 0.057)	C552	1.1	C552	0.5	4.4	2.025	6.0	Y
A14 (g, 0.016)	C552	1.0	SPC	0.165	1.5	2.0	2.0	Y
T14 (h, 0.016)	A150	1.0	SPC	0.165	1.5	2.0	2.0	Y
A14SL (g, 0.016)	C552	1.1	SPC	0.165	1.5	2.025	2.0	Y
A16 (g, 0.007)	C552	0.5	SPC	0.165	1.3	1.2	2.4	Y
			PTW					
30010 (e, 0.6)	PMMA/Gr	0.335/0.09	Al	0.55	20.4	3.05	23.4	N
30011 (d, 0.6)	Gr	0.425	Gr	0.5	20.4	3.05	23.4	N
30012 (c, 0.6)	Gr	0.425	Al	0.55	20.4	3.05	23.4	N
30013 (e, 0.6)	PMMA/Gr	0.335/0.09	Al	0.55	20.5	3.05	23.4	Y
31010 (e, 0.125)	PMMA/Gr	0.55/0.15	Al	0.55	6.0	2.75	6.5	Y
31016 (i, 0.016)	PMMA/Gr	0.57/0.09	Al	0.09	1.45	1.45	2.9	Y
31014 (i, 0.015)	PMMA/Gr	0.57/0.09	Al	0.09	4.0	1.0	5.0	Y
			IBA					
FC65-G (c, 0.65)	Gr	0.43	Al	0.5	21.3	3.1	23.1	Y
FC65-P (f, 0.65)	POM	0.4	Al	0.5	21.3	3.1	23.1	Y
CC25 (a, 0.25)	C552	0.4	C552	0.5	7.6	3.0	10.0	Y
FC23-C (a, 0.23)	C552	0.4	C552	0.5	7.0	3.1	8.8	Y
CC13 (a, 0.13)	C552	0.4	C552	0.5	3.2	3.0	5.8	Y
CC08 (a, 0.08)	C552	0.4	C552	0.5	1.4	3.0	4.0	Y
CC04 (a, 0.04)	C552	0.4	C552	0.5	2.5	2.0	3.6	Y
CC01 (g, 0.01)	C552	0.5	Steel	0.175	2.7	1.0	3.6	Y
			Other					
NE2581 (b, 0.6)	A150	0.36	A150	1.5	20.5	3.15	24.0	N
NE2571 (c, 0.6)	Gr	0.36	Al	0.5	20.5	3.14	24.0	N
NE2561 (c, 0.325)	Gr	0.53	Al	0.5	5.2	3.7	8.9	N
Capintec PR06C/G (a, 0.65)	C552	0.28	C552	0.8	22.0	3.22	24.0	N

(PMMA) sleeve is added to the model for a more realistic simulation, although these were not included in calculations done for TG-51.[17] Calculations were performed for the NE2571 with a 0.5 mm air gap between the sleeve and the chamber; the effect on D_{ch} is less than 0.15% compared to calculations without an air gap. Each chamber is loosely placed into one of nine groups, referenced by the letters a–i. The chambers are grouped by wall material, central electrode material, and chamber volume, as given in Table I. Grouping the chambers in this way allows a dissection of the differences between Monte Carlo calculated values and those provided in protocols. In order to explain the differences between k_Q values calculated with Monte Carlo and those used in TG-51, the ratio $[(P_{\text{wall}})^Q_{\text{Co}}]^{\text{TG51}}_{\text{MC}}$ is calculated for the various wall materials used in this study using previously described methods.[3] Values of P_{wall} calculated here show a negligible difference from those in the work of Buckley and Rogers.[3]

In order to calculate k_Q values to a relative uncertainty of 0.1%, the relative uncertainty on the individual calculations

TABLE II. The radiation sources and beam quality specifiers; the photon component of the percentage depth-dose at 10 cm for a 10×10 cm^2 field on the surface of the water phantom, $\%dd(10)_x$, and the tissue-phantom ratio at 20 and 10 cm, TPR_{10}^{20}, calculated with the formula of Kalach and Rogers (Ref. 22) The relative statistical uncertainty of the $\%dd(10)_x$ calculations is 0.1%.

Beam	Nominal energy (MV)	$\%dd(10)_x$	TPR_{10}^{20}
^{60}Co Eldorado 6[a]	···	58.4	0.569
Siemens KD[b]	6	67.0	0.671
	18	77.7	0.762
Elekta SL25[b]	6	67.3	0.672
	25	82.8	0.791
Varian Clinac[b]	4	62.7	0.623
	6	66.5	0.666
	10	73.8	0.734
	15	77.8	0.763
	18	81.5	0.785
Varian Clinac[c]	24	86.1	0.805

[a]Reference 18.
[b]Reference 19.
[c]Reference 20.

of absorbed dose must be less than 0.05%. This requires a significant amount of computing time especially for the chambers with a very small volume. The time required for computation also varies with beam energy. Cobalt-60 calculations require about one fifth of the CPU time required for the highest energy beam using appropriate cross-section enhancement factors. The time dependence on volume, V, scales as approximately $1/\sqrt{V}$. In the worst case scenario, the computing time is about 800 h on a single 3 GHz Woodcrest CPU for the calculation of the absorbed dose-to-air in the smallest ion chambers (IBA CC01 and Exradin A16) in the highest energy beam.

For some chambers, TG-51 k_Q values are not available as a comparison to Monte Carlo calculated values. In these cases, the program used for TG-51 calculations, prot51, is used to calculate k_Q values.[17] This program can calculate k_Q values for chambers with an aluminum electrode with a radius of 0.5 mm or without an electrode. Consequently, for the chambers with electrodes made of other metals, it is unclear which option to choose. In these cases, prot51 calculations are done with and without a 0.5 mm aluminum electrode.

II.B. Radiation sources and beam quality specifiers

The beams that are used in the simulations are modeled using tabulated spectra from previous publications.[18–20] The spectra used are listed in Table II along with the original references and our calculated beam quality specifiers. In this work, the beam quality specifiers are the photon component of the percent depth-dose at 10 cm depth in a 10×10 cm^2 field at the surface, $\%dd(10)_x$, and the tissue-phantom ratio at 20 and 10 cm for a 10×10 cm^2 field at the depth of measurement, TPR_{10}^{20}. The value of $\%dd(10)_x$ is calculated for each spectrum using BEAMnrc.[21] The absorbed dose-to-water is calculated along the central axis of a cylindrical water phantom in individual disks of water with thicknesses of 0.2 cm and radii of 0.5 cm. The water phantom itself is a cylinder with a radius of 20 cm and a thickness of 30 cm. The beam is modeled as a point source with the tabulated spectra and collimated into a 10×10 cm^2 field on the surface of the water phantom at an SSD of 100 cm, as recommended by TG-51.[1] The calculated $\%dd(10)_x$ values are given in Table II and they differ by less than 0.2% from the results of Kalach and Rogers.[22] The analytical expression, given by Kalach and Rogers,[22] which applies to flattened clinical accelerator beams, is used to convert from $\%dd(10)_x$ to TPR_{10}^{20}. The values of TPR_{10}^{20} are also listed in Table II.

II.C. Systematic uncertainties

Despite the low relative statistical uncertainty that can be achieved by simply increasing the number of histories, there exist several sources of systematic uncertainty in the calculation of k_Q. Systematic uncertainties arise from uncertainties in photon cross-sections, stopping powers, chamber dimensions, the use of photon spectra instead of full linac head models, and possible variation of W/e with beam energy. It is possible to investigate most of these effects using different methods in egs_chamber. In the energy range of interest, the photon's incoherent scattering cross-section is the most relevant. The estimated uncertainty in this cross-section is less than 1%–2%.[23] Thus, to study the uncertainty introduced by photon cross-sections, the "scale photon x-sections" utility in egs_chamber is used to change the photon cross-sections for each material by 1%. If photon cross-section uncertainties are uncorrelated, then the photon cross-sections must be scaled separately for each material. When investigating changes in k_Q from changes in the cross-sections for the air, wall, and electrode materials, the component of k_Q from the dose-to-water need not be considered and variations in k_Q are proportional to $(D_{ch})_Q^{^{60}\mathrm{Co}}$. Correlated sampling is used to dramatically decrease the relative statistical uncertainty on dose ratios. Simulations of two identical chambers are performed with the photon cross-sections for the material of interest in one of the chambers scaled by 1%. The egs_chamber code calculates R_{ch}, the ratio of the dose-to-air from the chamber with scaled cross-sections, and the chamber with default cross-sections. Then the relative uncertainty in k_Q (Δk_Q) in percent, is given by

$$\Delta k_Q = \left| \frac{R_{ch}(^{60}\mathrm{Co})}{R_{ch}(Q)} - 1 \right| \times 100\%. \quad (4)$$

The situation is more complicated when calculating the uncertainty in k_Q when varying the photon cross-sections for the water phantom. In this case, the entire phantom must be considered as a correlated geometry. To investigate this effect, the entire water phantom is surrounded by a 1 mm layer of air. Histories begin at the surface of the air (as if coming from the point source) and the calculations are performed using correlated sampling from the surface of the water. The use of the outer layer of air is required to employ correlated sampling in egs_chamber. Four geometries are modeled for

one simulation in one beam. The first two geometries calculate the dose-to-air in the chamber in the phantom with the default and the scaled photon cross-sections for water to obtain $R_{ch}(Q)$. The other two geometries calculate the dose-to-water at the reference point in the phantom with the default and the scaled photon cross-sections to obtain $R_w(Q)$. When using correlated sampling in the egs_chamber code, all geometries must be the same but the materials can be changed. In order to put this into practice, the dose-to-water is calculated by changing all of the chamber materials to water and then scoring the dose in each of the cavity and electrode chamber regions. Finally, Δk_Q is calculated, in percent, using

$$\Delta k_Q = \left| \left(\frac{R_w}{R_{ch}} \right)^{Q}_{^{60}\mathrm{Co}} - 1 \right| \times 100\%. \quad (5)$$

Calculations of Δk_Q are performed after scaling photon cross-sections for graphite and water in three beams, namely, in the Varian 4, 10, and 18 MV beams. It is confirmed that the largest change in k_Q is for the calculations with the Varian 18 MV beam. For all materials other than graphite and water, Δk_Q is calculated using this beam quality.

Another way to calculate k_Q is to consider correlations in the ratio D_w/D_{ch} and do the calculation separately with the different cross-sections, yielding a relative uncertainty in k_Q given by

$$\Delta k_Q = \left| \left[\left(\frac{D_w}{D_{ch}} \right)^{Q}_{^{60}\mathrm{Co}} \right]^{\mathrm{scaled}}_{\mathrm{default}} - 1 \right| \times 100\%. \quad (6)$$

In fact, one can ignore the correlations altogether in the calculations and calculate the required doses in eight separate calculations. All three methods give the same result at the 0.1% level for Δk_Q; however, the statistical precision for a given number of histories is much better using correlated sampling for at least part of the calculation.

Since calculations of photon incoherent cross-sections are based on the same theoretical models for all low-Z materials[24] it is reasonable to assume that photon cross-sections are correlated. If the theory is wrong by 1% then the photon cross-sections will likely change in the same direction and it is thought that the effect will cancel for dose ratios. For example, although there are uncertainties in the mass attenuation coefficient, μ/ρ, of the order of 1%, when standards laboratories assess the uncertainty on $(\mu_{\mathrm{en}}/\rho)^{\mathrm{gr}}_{\mathrm{air}}$, values as low as 0.04% are used.[25] To determine the uncertainty on k_Q in the case of correlated changes, k_Q is calculated after scaling the cross-sections for all materials by 1% in the same direction for three beam qualities and the uncertainty on k_Q is taken as the maximum variation in k_Q. Another way of investigating correlated uncertainties is to change certain Monte Carlo transport parameters to vary cross-sections. As Compton scattering is the most important interaction in this energy range, the Compton Monte Carlo transport parameters are the most relevant so the effect of using different Compton options is tested, although the effect on photon cross-sections is small in this energy range. Values of k_Q are calculated with bound Compton scattering turned on and radiative Compton corrections off, both options on, and both options off. Varying these options cause changes in k_Q of about 0.1% for the materials and energy range of interest.

The uncertainty in k_Q due to uncertainty in electron stopping powers is studied by varying the mean excitation energy, I, for each material, which is likely the largest source of uncertainty. Uncertainties on I-values are given in ICRU Report 37 for common materials.[26] For each material, density files are created using the ESTAR program with I-values corresponding to the upper and lower one standard deviation limits from ICRU Report 37. If a given material is not listed in ICRU Report 37, a nominal value of 5% is taken as the one standard deviation uncertainty in the I-value. Δk_Q is then calculated for chambers using the same approach described above for photon cross-sections. In these simulations, $R_{ch}(Q)$ is calculated as the ratio of the dose-to-air for the chamber with the stopping power varied for the material of interest to that using default stopping powers. The same approach is taken to investigate the uncertainty from changing the water stopping power as that used for photon cross-sections. There is also some uncertainty due to the density effect used, especially for ^{60}Co beams. However, the variation in stopping power due to this is about one seventh that due to the I-value[27] at ^{60}Co energies and is therefore negligible and ignored.

Calculations of Δk_Q are performed by applying uncertainties in photon cross-sections and electron stopping powers in both directions for the water phantom and graphite and C552-walled chambers. It is found that the uncertainty interval is symmetric within the relative statistical uncertainty of Δk_Q calculations (0.05%).

Uncertainty is introduced in calculated k_Q factors when exact chamber dimensions are not known. Variations in wall thickness and the exact dimensions of the air cavity probably introduce the most uncertainty in k_Q calculations. Uncertainty in k_Q from the variation in wall thickness is calculated using the Exradin A12, the NE2571, and the PTW 30013 chambers to represent chambers with C552, graphite, and PMMA walls, respectively. The uncertainty in k_Q is also determined for the PTW 31014 ion chamber when varying the wall thickness to quantify the effect for small-volume chambers. For each of these chambers, the wall thickness is varied by $\pm 5\%$, keeping the cavity volume unchanged, and k_Q is calculated for three beam qualities using the Varian Clinac 4, 10, and 18 MV spectra as representative low, medium, and high-energy beams. The maximum relative percent difference in k_Q is taken as a conservative estimate of the uncertainty.

In Fig. 3 of Wang and Rogers,[5] P_{repl} values are plotted as a function of cavity radius for an 18 MV beam with $\%dd(10)_x = 82\%$ and a cobalt-60 source. The ratio of these P_{repl} values is calculated at each radius, yielding $(P_{\mathrm{repl}})^{Q}_{\mathrm{Co}}$. A linear fit to the $(P_{\mathrm{repl}})^{Q}_{\mathrm{Co}}$ data as a function of radius is made to determine the rate of change of k_Q as a function of cavity radius. The uncertainty on k_Q due to the uncertainty in cavity

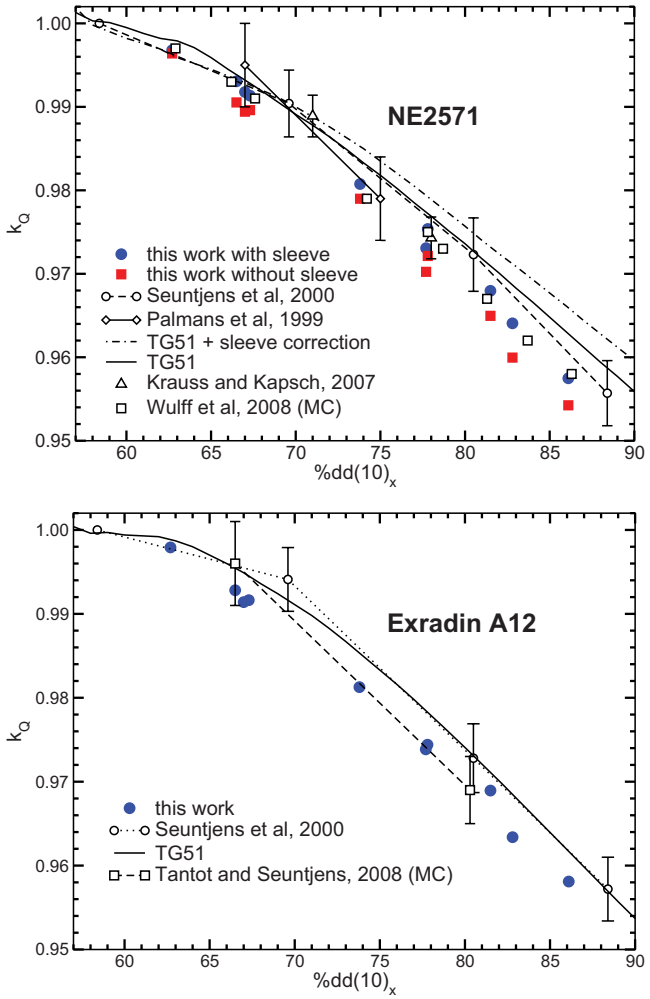

FIG. 2. Comparison of k_Q calculations with experimental and Monte Carlo data for the NE2571 and Exradin A12 chambers. The experimental data are from Seuntjens *et al.* (Ref. 8), Palmans *et al.* (Ref. 10), and Krauss and Kapsch (Ref. 9), while the Monte Carlo data are from Wulff *et al.* (Ref. 4) and Tantot and Seuntjens (Ref. 7). The relative statistical uncertainties on the calculations in this work are smaller than the symbols.

dimensions is estimated by multiplying the slope of the linear fit by the uncertainty in cavity radius, taken to be ±5% of a typical farmer chamber radius (3 mm).

The use of photon spectra to define the radiation sources instead of using a full BEAMnrc model adds systematic uncertainty in k_Q. This is quantified using full BEAMnrc models of the Varian 18 MV, Elekta SL25 6 MV, and ^{60}Co Eldorado 6 to create phase-space files for use as a source and using the same simulations to obtain a spectrum file for the source input. Additionally, there are multiple choices of spectra available for the cobalt-60 source. The effect of using a different spectrum is tested by calculating D_w/D_{ch} using each cobalt-60 spectrum as well as a monoenergetic 1.25 MeV beam for various chambers.

The results for systematic uncertainties are combined following the same procedure used by Wulff *et al.*[28] based on the familiar equation for combined standard uncertainty:

$$u_{k_Q} = \left[\sum_{i=1}^{n} \left(\frac{\partial k_Q}{\partial x_i} \right)^2 u^2(x_i) \right]^{1/2}, \quad (7)$$

where $u(x_i)$ represents the systematic uncertainty on the variable in question. This equation can be simplified by approximating $\partial k_Q/\partial x_i$ by $\Delta k_Q/\Delta x_i$ and calculating the change in k_Q (Δk_Q) when $\Delta x_i = u(x_i)$. Equation (7) becomes

$$u_{k_Q} = \left[\sum_{i=1}^{n} (\Delta k_Q)_i^2 \right]^{1/2}, \quad (8)$$

so that the combined uncertainty in k_Q is the sum of the squared variations in k_Q when each of the variables in question is changed by one standard deviation.

III. RESULTS AND DISCUSSION

III.A. Comparison to other studies

Figure 2 provides the results of Monte Carlo calculations along with the experimental and previous Monte Carlo calculations for the NE2571 and Exradin A12 chambers. The present NE2571 calculations with a PMMA sleeve are in excellent agreement with all three sets of experimental results and previous Monte Carlo calculations from Wulff *et al.*[4] The Exradin A12 calculations agree within one standard deviation with the experimental results of Seuntjens *et al.*[8] and Monte Carlo calculations from Tantot and Seuntjens.[7]

The results from this study are compared to Monte Carlo calculations from González-Castaño *et al.*,[6] although the comparison is not explicitly shown. There is agreement within one standard deviation for the PTW 30013, PTW 31010, Exradin A1Sl, and Exradin A14SL chambers although the relative uncertainties on the calculations in that study are between 0.5% and 1% compared to 0.1% here. The two sets of calculations for the PTW 31014 and IBA CC04 exhibit a maximum difference of 1%. In the case of the PTW 31014 calculations, the results of González-Castãno are always higher than those from this study by about 0.7%. The CC04 calculations are in fairly good agreement except for one point in the high-energy range that lies outside of one standard deviation. The largest difference between the two data sets is for simulations of the IBA CC01 chamber with a maximum percent difference of 2%. Almost all points lie outside of one standard deviation, suggesting significant differences between the two chamber models. This is not evident from the tabulated values of chamber dimensions in that study, although the radii and lengths of the electrodes, which are critical in small chambers, are not given by González-Castaño *et al.*[6] (although private communications have indicated no significant geometric differences).

Figure 3 provides a subset of the calculated values compared to the TG-51 or TG-51 equivalent values calculated with prot51. The subset is chosen so that each representative chamber group from Table I is characterized. A polynomial fit to the data as a function of beam quality of the form

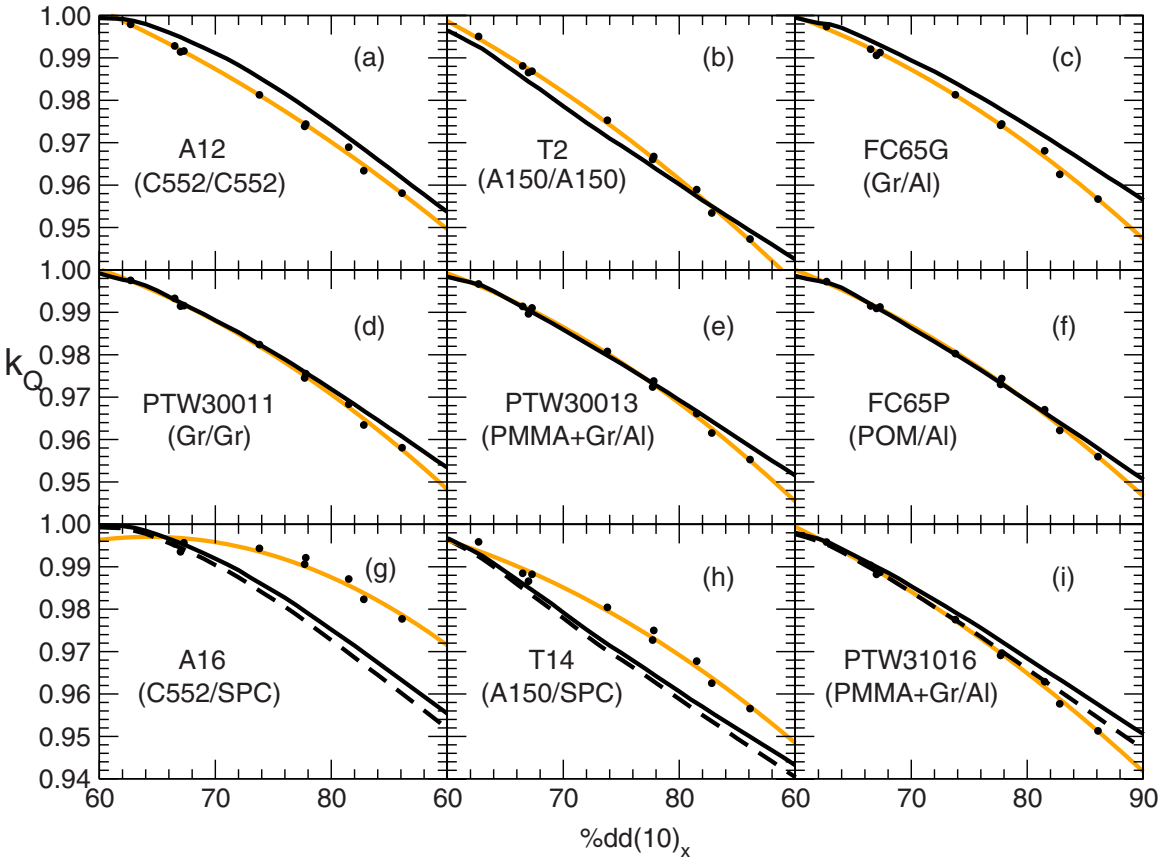

FIG. 3. Representative Monte Carlo calculated k_Q values (solid points) along with a fit to the data (light-colored lines) and the TG-51 calculated values (black lines). The chambers with small cavities and metal electrodes have two sets of TG-51 calculated values, one with a 0.5 mm radius aluminum electrode (solid black lines) and another without (dashed lines). The chamber that is used as a representative is given along with a brief classification given as (wall/electrode material).

$$k_Q = a + b(\%dd(10)_x) + c(\%dd(10)_x)^2, \qquad \%dd(10)_x \geq 62.7\% \tag{9}$$

is done for each chamber. The fitting parameters, a, b, and c, and the root mean square deviation are given in Table III. For $\%dd(10)_x < 62.7\%$, one should extrapolate linearly to unity for ^{60}Co beams.

Figure 4 provides a subset of calculated k_Q values as a function of TPR_{10}^{20} along with values from TRS-398 [2] where those values are available. The same representative chamber group is used as in Fig. 3. A polynomial fit to the data as a function of TPR_{10}^{20} of the form

$$k_Q = a' + b'(\mathrm{TPR}_{10}^{20}) + c'(\mathrm{TPR}_{10}^{20})^2 + d'(\mathrm{TPR}_{10}^{20})^3, \qquad \mathrm{TPR}_{10}^{20} \geq 0.623 \tag{10}$$

is done for each chamber. The fitting parameters, a', b', c', and d', and the root mean square deviation (typically less than 0.1%) are given in Table III. The comparison between Monte Carlo calculated and TG-51 k_Q values that follows is not done for TRS-398 values because the individual correction factors used there are not always available.

The correction factors used by TG-51 in Eq. (2) account for the differences between k_Q values calculated in this work and TG-51. In Farmer-type chambers at higher energies, the TG-51 $(P_{\mathrm{repl}})_{\mathrm{Co}}^{Q}$ values are up to 0.2% higher than the more accurate values calculated by Wang and Rogers.[5] Thus, variation in $(P_{\mathrm{repl}})_{\mathrm{Co}}^{Q}$ results in a higher k_Q value in TG-51 calculations for all chambers at high energy. The difference between this study and TG-51 values due to variations in wall and central electrode effects depends on the type of chamber. Figure 5 shows the ratio of $[(P_{\mathrm{wall}})_{\mathrm{Co}}^{Q}]_{\mathrm{MC}}^{\mathrm{TG51}}$ for the various wall materials used in this study. This plot allows an analysis of the differences between TG-51 k_Q values and those calculated with Monte Carlo simulations. If the ratio is greater than 1, then the TG-51 calculations would be higher than the Monte Carlo calculations and vice versa.

For group (a) chambers with C552 walls and central electrode, the differences between these calculations and TG-51 values seen in Fig. 3 are caused by a high $(P_{\mathrm{wall}})_{\mathrm{Co}}^{Q}$ ratio in TG-51. The central electrode does not result in a significant effect because it is composed of the same material as the wall.

Chambers in group (b) are those with A150 walls and central electrodes. The TG-51 k_Q values are lower than the Monte Carlo calculations in the low-energy range and higher at high energies. In the low-energy range, the difference is explained by the $[(P_{\mathrm{wall}})_{\mathrm{Co}}^{Q}]_{\mathrm{MC}}^{\mathrm{TG51}}$ ratio for the T2 chamber in

TABLE III. Fitting parameters for Eq. (9) for k_Q in terms of $\%dd(10)_x$ (a, b, c) and Eq. (10) in terms of TPR_{10}^{20} (a', b', c', d'). The rms deviation of the data from the fits are also given. The fits to Eq. (9) are valid for values of $\%dd(10)_x$ between 62.7% and 86.1%. The fits to Eq. (10) are valid for values of TPR_{10}^{20} between 0.623 and 0.805. For clarity, b for the A12 is 0.777×10^{-3}.

Chamber	a	b ($\times10^3$)	c ($\times10^5$)	rms % deviation	a'	b'	c'	d'	rms % deviation
				Exradin					
A12	1.0146	0.777	−1.666	0.07	2.6402	-7.2304	10.7573	-5.4294	0.08
A19	0.9934	1.384	−2.125	0.04	3.0907	-9.1930	13.5957	-6.7969	0.05
A2	0.9819	1.609	−2.184	0.07	2.8458	-8.1619	12.1411	-6.1041	0.07
T2	1.0173	0.854	−1.941	0.07	3.3433	-10.2649	15.1247	-7.5415	0.07
A12S	0.9692	1.974	−2.448	0.07	2.9597	-8.6777	12.9155	-6.4903	0.07
A18	0.9944	1.286	−1.980	0.06	2.5167	-6.7567	10.1519	-5.1709	0.07
A1	1.0029	1.023	−1.803	0.06	2.0848	-4.9174	7.5446	-3.9441	0.07
T1	1.0552	−0.196	−1.275	0.06	2.8060	-7.9273	11.7541	-5.9263	0.08
A1SL	0.9896	1.410	−2.049	0.08	2.8029	-7.9648	11.8445	-5.9568	0.08
A14	0.9285	2.706	−2.599	0.2	5.4677	-19.1795	27.4542	-13.1336	0.07
T14	0.9622	2.009	−2.401	0.1	4.9690	-17.1074	24.6292	-11.8877	0.09
A14SL	0.9017	3.454	−3.083	0.2	5.1205	-17.7884	25.6123	-12.3232	0.08
A16	0.8367	4.987	−3.877	0.2	6.0571	−21.7829	31.2289	-14.9168	0.09
				PTW					
30010	1.0093	0.926	−1.771	0.08	2.5318	-6.7948	10.1779	-5.1746	0.08
30011	0.9676	2.061	−2.528	0.07	2.9044	-8.4576	12.6339	-6.3742	0.07
30012	0.9537	2.440	−2.750	0.04	3.2836	-10.0610	14.8867	-7.4212	0.05
30013	0.9652	2.141	−2.623	0.07	3.2012	-9.7211	14.4211	-7.2184	0.07
31010	0.9590	2.265	−2.684	0.05	3.1578	-9.5422	14.1676	-7.0964	0.06
31016	1.0085	1.028	−1.968	0.07	2.9524	-8.6054	12.7757	-6.4265	0.08
31014	1.0071	1.048	−1.967	0.06	3.0178	-8.8735	13.1372	-6.5867	0.08
				IBA					
FC65-G	0.9708	1.972	−2.480	0.07	3.3221	-10.2012	15.0497	-7.4872	0.08
FC65-P	0.9828	1.664	−2.296	0.07	3.0872	-9.1919	13.6137	-6.8118	0.08
CC25	0.9551	2.353	−2.687	0.06	2.4567	-6.5932	10.0471	-5.1775	0.06
FC23-C	0.9820	1.579	−2.166	0.06	3.0511	-9.0243	13.3378	-6.6559	0.06
CC13	0.9515	2.455	−2.768	0.06	3.1982	-9.7182	14.4210	-7.2121	0.06
CC08	0.9430	2.637	−2.884	0.09	3.7328	-11.9800	17.5884	-8.6843	0.08
CC04	0.9714	1.938	−2.432	0.08	3.0054	-8.8633	13.1704	-6.6075	0.08
CC01	0.9116	3.358	−3.177	0.1	4.3376	-14.4935	21.0293	-10.2208	0.05
				Other					
NE2581	1.0318	0.488	−1.731	0.07	2.9190	-8.4561	12.5690	-6.3468	0.08
NE2571	0.9882	1.486	−2.140	0.07	2.2328	-5.5779	8.5325	-4.4352	0.09
NE2561	1.0200	0.596	−1.551	0.09	2.4235	-6.3179	9.4737	-4.8307	0.09
Capintec PR06C/G	0.9519	2.432	−2.704	0.07	2.9110	-8.4916	12.6817	-6.3874	0.08

Fig. 5. In the high-energy range, where this ratio is close to unity, the TG-51 k_Q result is higher because of the higher values of $(P_{repl})^Q_{Co}$ used in TG-51. Again, the central electrode does not result in a significant variation between the two results.

For group (c) chambers with graphite walls and an aluminum central electrode, the calculated values are in agreement with TG-51 values at low energies with a larger difference as the $\%dd(10)_x$ is increased. The difference arises from the wall correction factors at high energies. The variation between the k_Q values can explained using the P_{wall} ratio for the NE2571 chamber in Fig. 5. For the chambers that are not waterproof in this group (NE2571 and PTW 30012), the effect of the waterproofing sleeve compensates for the difference between the two data sets by as much as 0.3%. The chamber used for this representative plot is inherently waterproof so this effect is not observed. Buckley *et al.*[29] showed that there is very little difference between their Monte Carlo calculated P_{cel} values and those in TG-51.

Chambers with a graphite wall and graphite central electrode, i.e., group (d), exhibit the same behavior as chambers in group (c). Again, there is very little difference between P_{cel} values used in TG-51 and calculated using Monte Carlo simulations.[29] In this case, the chamber is not inherently waterproof so the improved agreement with TG-51 is due to the compensating effect of the PMMA sleeve in the Monte Carlo calculations.

For group (e), chambers with PMMA and graphite walls and an aluminum central electrode, the k_Q values agree in the low-energy range, but at higher energies the TG-51 values

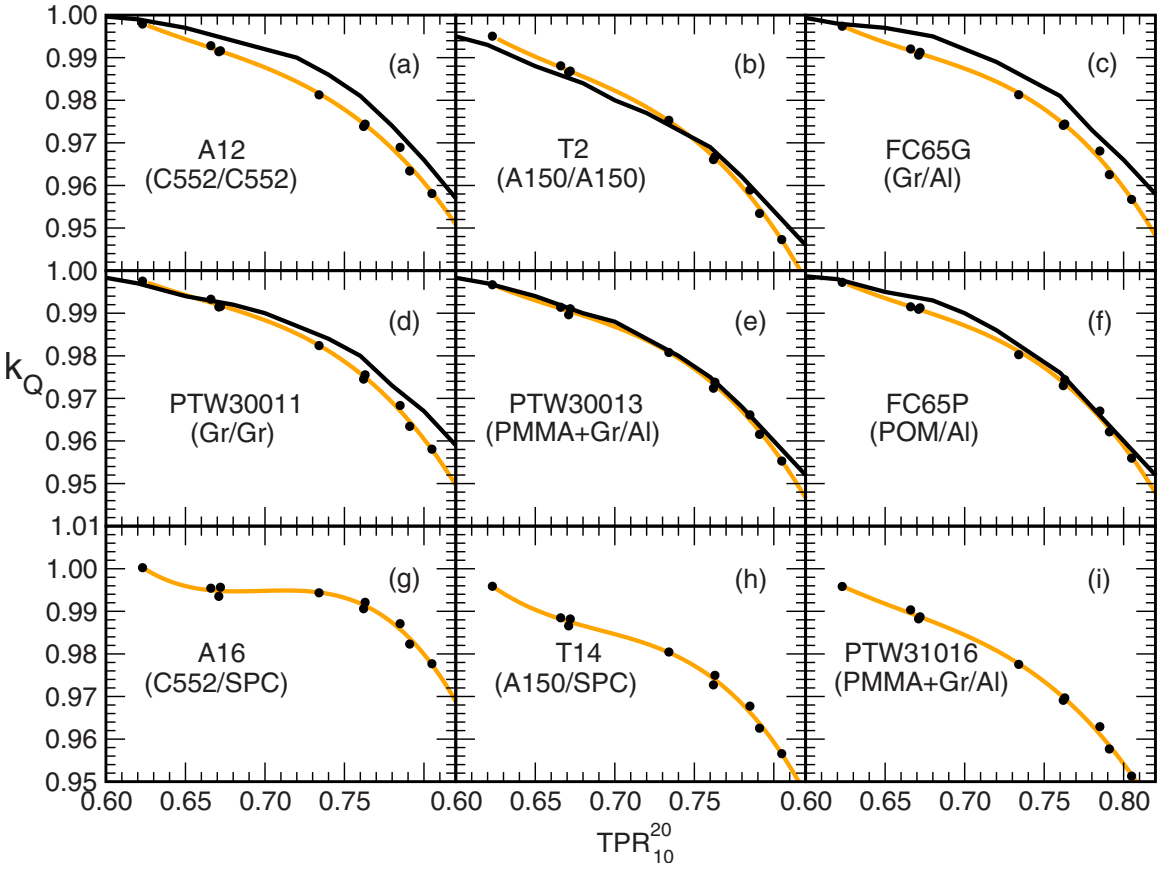

FIG. 4. Representative Monte Carlo calculated k_Q values (solid points) along with a fit to the data (light-colored lines) and the TRS-398 calculated values (where available, black lines) as a function of TPR^{20}_{10}. The chamber that is used as a representative is given along with a brief classification given as (wall/electrode material).

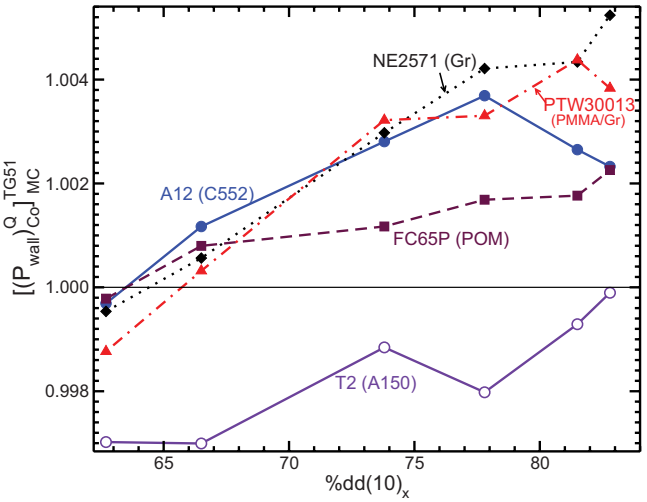

FIG. 5. The ratio of $(P_{wall})^Q_{Co}$ values used in TG-51 to the more accurate values calculated using Monte Carlo simulations. The ratios are a function of wall thickness and thus specific to the chambers mentioned, although the differences for chambers with the same wall materials are explained using the ratios from this plot. Multiplying Monte Carlo calculated k_Q values by these ratios indicate what the value of k_Q would be if TG-51 values of P_{wall} were used.

are higher than those calculated here. The difference in P_{wall} values is partially compensated by the sleeve effect. The most significant difference results from the effect of incorrect P_{repl} values used in TG-51 at high energies.

Chambers of group (f), with a polyoxymethylene [(POM) trade name Delrin] wall and an aluminum central electrode, exhibit similar behavior to TG-51 values with a slight deviation as $\%dd(10)_x$ increases. Again, this difference is caused by the variation of P_{wall} and P_{repl} values. The result for the FC65P chamber in Fig. 5 shows that the P_{wall} values agree at low energies but as the energy is increased the two values differ by as much as 0.2%.

Small-volume chambers (<0.02 cm^3) with C552 walls and electrodes made from high-Z materials [silver plated copper covered steel (SPC) or steel], group (g), exhibit the most rms variation about the quadratic fit and from a TG-51 calculation without an electrode. Calculating k_Q for the Exradin A16 chamber without a central electrode in the Monte Carlo model shows better agreement with the values calculated with the TG-51 program prot51. This suggests that the correction for the central electrode is very large for these chambers. The remaining difference arises from the difference in P_{wall} values for C552 in the two approaches. The prot51 calculations with a 1 mm diameter aluminum electrode are in better agreement with the Monte Carlo calculations performed with a high-Z electrode.

TABLE IV. Uncertainties in k_Q, in percent, due to variations in photon cross-sections and electron stopping powers. Photon cross-sections are varied separately for each material by 1%. Electron stopping powers are varied by changing the mean excitation energy, I, for each material separately. The first column shows the percent variation in I values used. The chambers used in each case are given in brackets. The relative statistical uncertainty in the calculations is less than 0.05%. This means that in cases where Δk_Q is less than 0.05%, the contribution to the uncertainty is negligible.

	Mean excitation energy		Photon cross-sections
Material	ΔI (%)	Δk_Q (%)	Δk_Q (%)
Water (NE2571)	1.5	0.03	0.55
C552 (Exradin A12)	5	0.30	0.53
Graphite Wall (NE2571)	4.5	0.19	0.29
PMMA (PTW 30013)	2	0.09	0.16
Air (NE2571)	2.5	0.03	0.02
Aluminum (NE2571)	0.5	0.00	0.01
POM/Delrin (IBA FC65P)	5	0.23	0.21
A150 (Exradin T2)	5	0.33	0.53
Steel Wire (IBA CC01)	5	0.01	0.05
SPC Electrode (Exradin A16)	5	0.03	0.02

For (h) type chambers with A150 walls and an SPC central electrode, the largest variation from TG-51 values is in the middle range of energies. The same central electrode effect occurs with these chambers as that observed for type (g) chambers. In the low-energy range, the results agree with TG-51 because the incorrect P_{wall} values used in TG-51 compensate for the central electrode effect. At higher energies, the replacement correction factor partially compensates for the effect of the central electrode. As exhibited by group (g) chambers, the prot51 calculations with an aluminum electrode differ less from Monte Carlo values than prot51 calculations without an electrode.

Finally, chambers with a PMMA and graphite wall and an aluminum central electrode, group (i), follow the same trend as Farmer-type chambers with the same wall and electrode materials (e). The agreement is very good between the Monte Carlo and TG-51 calculations. This agreement for very short group (i) chambers verifies the result of Wang and Rogers[5] that the replacement correction factor varies by less than 0.2% as a function of cavity length as TG-51 calculations use P_{repl} values for a 24 mm long chamber.

III.B. Systematic uncertainties

The relative statistical uncertainty in calculated k_Q factors is less than 0.1% but systematic uncertainties can play a significant role. When calculating ion chamber response, EGSnrc has been shown to be accurate to within 0.1% with respect to its own cross-sections.[30] If the uncertainties in the photon cross-sections are taken to be uncorrelated, the results are given in Table IV. Note that materials with a large variation in P_{wall} values with beam quality introduce a larger uncertainty in k_Q from photon cross-section uncertainties. For the more likely situation that photon cross-section uncertainties are correlated, the uncertainty in k_Q when all of the photon cross-sections are scaled by the same amount in the same direction is negligible. The effect of varying the Compton options results in k_Q values which are all unchanged within the statistical uncertainty of 0.1%. Uncertainties in stopping powers introduce the uncertainties in k_Q provided in Table IV. As a conservative limit, these are assumed to be uncorrelated since the values of I are measured independently, although using similar techniques which may introduce some correlation. The maximum variation in k_Q when changing the wall thickness by 5% is 0.1% for both PMMA-walled chambers investigated so, as a conservative estimate, a 0.1% uncertainty is applied for all chambers. Using the method described in Sec. II B and the P_{repl} calculations as a function of cavity radius by Wang and Rogers,[5] Δk_Q is found to be 0.005% due to uncertainty in air cavity dimensions. This is negligible compared to the statistical uncertainty on P_{repl} calculations from that work. The difference in k_Q values calculated using a full BEAMnrc model and a spectrum file as a source input as described in Sec. II C is less than 0.1%. For the standard Farmer-type chambers, using a monoenergetic 1.25 MeV beam for the cobalt-60 source gives a D_w/D_{ch} ratio that is within 0.1% of the result calculated with a beam modeled from a realistic spectrum. However, for small chambers with electrodes made of high-Z materials, the D_w/D_{ch} ratios calculated with realistic cobalt-60 spectra differ by 1% from the result calculated with a monoenergetic 1.25 MeV beam. Nonetheless, the results for the various realistic spectra are all unchanged within the statistical uncertainty of 0.1%.

Equation (3) is valid if W/e is assumed constant across the range of beam energy used for the calculations. There is evidence that this is not correct. In Ref. 30, the value of W/e for a monoenergetic electron beam is estimated to vary by about 0.5 eV over the entire range of energies from 0 to about 40 MeV.[31] This leads to a ± 0.25 eV, or 0.75%, uncertainty in W/e. This is an upper limit for the uncertainty on W/e especially as the experiment for electron beams is actually looking at $w(E)/e$, i.e., the energy lost per Coulomb of charge released by electrons of a certain energy. In photon beams, we are interested in W/e for the entire slowing down spectrum of electrons which will be much less sensitive to these variations in $w(E)/e$. In TRS-398, an uncertainty of 0.5% is assigned to k_Q from uncertainty in this component.[2] This uncertainty is large and deserves further investigation but the value given in TRS-398 is used here.

For a chamber in group (c), which includes the NE2571 and PTW 30012 chambers, the various sources of uncertainty, x_i, the uncertainty in the variable, $u(x_i)$, and the corresponding uncertainty in k_Q, $\Delta(k_Q)_i$, are listed in Table V, along with the final systematic uncertainty in k_Q obtained using Eq. (7) with and without including correlated photon cross-sections and the uncertainty on W/e. Our results for uncorrelated and correlated photon cross-sections without W/e are roughly comparable to those of Wulff *et al.*,[28] viz., 0.40% and 0.95%, although there are many small differences on individual components and they completely ignore the variation in W/e. The systematic uncertainty in k_Q due to

TABLE V. The relative change in each variable $u(x_i)$, contributing a component to the systematic relative uncertainty $\Delta(k_Q)_i$, for an ion chamber in group c (NE2571-graphite wall, Al electrode). Values are in percent. The uncertainty in k_Q from correlated photon cross-section uncertainties is negligible.

Variable, x_i	$u(x_i)$ (%)	$\Delta(k_Q)_i$ (%)
Mean excitation energy, I		
Water	1.5	0.03
Air	2.5	0.03
Graphite wall	4.5	0.19
Aluminum electrode	0.5	0.00
Photon cross-sections		
Water	1.0	0.55
Air	1.0	0.03
Graphite wall	1.0	0.29
Aluminum electrode	1.0	0.01
All (correlated)	1.0	0.0
Other sources		
Statistical uncertainty	⋯	0.1
EGSnrc[a]	⋯	0.1
Wall thickness	5.0	0.1
Cavity dimensions	5.0	0.00
Source model	⋯	0.1
W/e	⋯	0.5
	u_{k_Q}	
Corr, no W/e	…	0.28
Uncorr, no W/e	…	0.68
Corr, with W/e	…	0.57
Uncorr, with W/e	…	0.85

[a]Reference 30.

variations in material parameters and the total systematic uncertainty in k_Q with and without correlated photon cross-sections and with and without the uncertainty in W/e are given for each chamber group in Table VI. The worst case uncertainty (uncorrelated photon cross-sections and with uncertainty due to W/e) is between 0.83 and 0.99% depending on the chamber materials.

Discussions with Roberto Capote raised concerns about the effects of correlation in the calculation of the ratio of D_w to D_{ch}. This is investigated by calculating this ratio using correlated sampling for two ionization chambers in two different beam qualities, namely, the NE2571 and the Exradin A12 chambers in ^{60}Co and the Varian 18 MV beams. It is found that within the 0.1% statistical uncertainty, the results do not change compared to two independent calculations of the same two doses but the relative statistical uncertainty is much lower due to the high degree of correlation in the geometries. The bulk of the k_Q values were determined in this work using the uncorrelated method so the statistical uncertainty may be higher than they could have been, but at 0.1% they are adequate in view of the larger systematic uncertainties. As discussed in Sec. II C, correlated sampling methods were used to improve the statistical precision, but they did not affect the calculated values of the uncertainties involved.

IV. CONCLUSIONS

With the availability of sophisticated variance reduction techniques and substantial computing power, it is now possible to calculate k_Q directly using Monte Carlo simulations. Calculated k_Q factors have been presented in terms of a high precision quadratic fit to the data for 32 ionization chambers. The differences between values calculated with the algorithm used by TG-51 and by Monte Carlo simulation have been highlighted and explained, mostly in terms of more accurate values for the P_{repl}, P_{cel}, and P_{wall} correction factors. Systematic uncertainties arise from a variety of sources and are very significant, especially the uncertainty in W/e which is common to both the TG-51 and Monte Carlo calculations of k_Q. Given the close agreement with most measurements, it seems likely that the systematic uncertainties are overestimated.

ACKNOWLEDGMENTS

The authors thank Joerg Wulff for making the egs_chamber user-code available before it was distributed with EGSnrc code system. The authors thank Brian Hooten of Standard Imaging for providing blueprints of Exradin ion chambers and Igor Gomola of IBA for providing technical drawings of the CC01 ion chamber. The authors thank Iwan

TABLE VI. The total systematic relative uncertainty in Monte Carlo calculated k_Q values, with and without correlated photon cross-section uncertainties and with and without the uncertainty on W/e, sorted by chamber group. The values are in percent.

	u_{k_Q}			
Group (Wall/Electrode)	Corr, no W/e	Uncorr, no W/e	Corr, with W/e	Uncorr, with W/e
a (C552/C552)	0.36	0.85	0.62	0.98
b (A150/A150)	0.39	0.86	0.63	0.99
c (Graphite/Al)	0.28	0.68	0.57	0.85
d (graphite/graphite)	0.28	0.68	0.57	0.85
e/i (PMMA+graphite/Al)	0.31	0.71	0.58	0.86
f (POM/Al)	0.32	0.66	0.59	0.83
g (C552/SPC)	0.36	0.85	0.62	0.98
h (A150/SPC)	0.39	0.86	0.63	0.99

Kawrakow for useful discussions about correlated uncertainties and Roberto Capote for useful discussions about correlated dose ratios. Thanks to Elsayed Ali, Rowan Thomson, and Justin Sutherland of the CLRP for helpful comments on the manuscript. This work is supported by an OGSST scholarship held by B.R. Muir, by NSERC, CRC program, CFI, and OIT.

[a]Electronic mail: bmuir@physics.carleton.ca
[b]Electronic mail: drogers@physics.carleton.ca

[1]P. R. Almond, P. J. Biggs, B. M. Coursey, W. F. Hanson, M. S. Huq, R. Nath, and D. W. O. Rogers, "AAPM's TG-51 protocol for clinical reference dosimetry of high-energy photon and electron beams," Med. Phys. **26**, 1847–1870 (1999).
[2]IAEA, "Absorbed dose determination in external beam radiotherapy: An international code of practice for dosimetry based on standards of absorbed dose to water, IAEA Technical Report Series No. 398 (IAEA, Vienna, 2001).
[3]L. A. Buckley and D. W. O. Rogers, "Wall correction factors, P_{wall}, for thimble ionization chambers," Med. Phys. **33**, 455–464 (2006).
[4]J. Wulff, J. T. Heverhagen, and K. Zink, "Monte-Carlo-based perturbation and beam quality correction factors for thimble ionization chambers in high-energy photon beams," Phys. Med. Biol. **53**, 2823–2836 (2008).
[5]L. L. W. Wang and D. W. O. Rogers, "The replacement correction factors for cylindrical chambers in high-energy photon beams," Phys. Med. Biol. **54**, 1609–1620 (2009).
[6]D. M. González-Castaño, G. H. Hartmann, F. Sanchez-Doblado, F. Gomez, R.-P. Kapsch, J. Pena, and R. Capote, "The determination of beam quality correction factors: Monte Carlo simulations and measurements," Phys. Med. Biol. **54**, 4723–4741 (2009).
[7]L. Tantot and J. P. Seuntjens, "Modeling ionization chamber response to nonstandard beam configurations," J. Phys. Conf. Ser. **102**, 012013 (2008).
[8]J. P. Seuntjens, C. K. Ross, K. R. Shortt, and D. W. O. Rogers, "Absorbed-dose beam quality conversion factors for cylindrical chambers in high-energy photon beams," Med. Phys. **27**, 2763–2779 (2000).
[9]A. Krauss and R.-P. Kapsch, "Calorimetric determination of k_Q factors for NE 2561 and NE 2571 ionization chambers in 5 cm×5 cm and 10 cm×10 cm radiotherapy beams of 8 MV and 16 MV photons," Phys. Med. Biol. **52**, 6243–6259 (2007).
[10]H. Palmans, W. Mondelaers, and H. Thierens, "Absorbed dose beam quality correction factors k_Q for the NE2571 chamber in a 5 MV and 10 MV photon beam," Phys. Med. Biol. **44**, 647–663 (1999).
[11]I. Kawrakow and D. W. O. Rogers, "The EGSnrc code system: Monte Carlo simulation of electron and photon transport," NRC Technical Report No. PIRS-701, v4-2-2-5 (National Research Council of Canada, Ottawa, Canada, 2007). See http://www.irs.inms.nrc.ca/inms/irs/EGSnrc/EGSnrc.html.
[12]I. Kawrakow, "Accurate condensed history Monte Carlo simulation of electron transport. I. EGSnrc, the new EGS4 version," Med. Phys. **27**, 485–498 (2000).
[13]J. Wulff, K. Zink, and I. Kawrakow, "Efficiency improvements for ion chamber calculations in high energy photon beams," Med. Phys. **35**, 1328–1336 (2008).
[14]I. Kawrakow, "egspp: The EGSnrc C++ class library," Technical Report No. PIRS-899 (National Research Council of Canada, Ottawa, Canada, 2005).
[15]E. G. A. Aird and F. T. Farmer, "The design of a thimble chamber for the Farmer dosemeter," Phys. Med. Biol. **17**, 169–174 (1972).
[16]D. J. La Russa, M. McEwen, and D. W. O. Rogers, "An experimental and computational investigation of the standard temperature-pressure correction factor for ion chambers in kilovoltage x rays," Med. Phys. **34**, 4690–4699 (2007).
[17]D. W. O. Rogers, in *Clinical Dosimetry Measurements in Radiotherapy*, edited by D. W. O. Rogers and J. E. Cygler (Medical Physics, Madison, 2009), pp. 239–296.
[18]G. Mora, A. Maio, and D. W. O. Rogers, "Monte Carlo simulation of a typical ^{60}Co therapy source," Med. Phys. **26**, 2494–2502 (1999).
[19]D. Sheikh-Bagheri and D. W. O. Rogers, "Monte Carlo calculation of nine megavoltage photon beam spectra using the BEAM code," Med. Phys. **29**, 391–402 (2002).
[20]R. Mohan, C. Chui, and L. Lidofsky, "Energy and angular distributions of photons from medical linear accelerators," Med. Phys. **12**, 592–597 (1985).
[21]D. W. O. Rogers, B. Walters, and I. Kawrakow, "BEAMnrc users manual," NRC Report No. PIRS 509(a), Rev. K, 2006.
[22]N. I. Kalach and D. W. O. Rogers, "Which accelerator photon beams are 'clinic-like' for reference dosimetry purposes?," Med. Phys. **30**, 1546–1555 (2003).
[23]J. H. Hubbell, "Review of photon interaction cross section data in the medical and biological context," Phys. Med. Biol. **44**, R1–R22 (1999).
[24]M. J. Berger, J. H. Hubbell, S. M. Seltzer, J. S. Coursey, and D. S. Zucker, "XCOM: Photon cross section database (version 1.2)," NIST Report No. NBSIR 87-3597 (NIST, Gaithersburg, MD, 1999). See http://physics.nist.gov/xcom.
[25]M. G. Mitch, L. A. DeWerd, R. Minniti, and J. F. Williamson, in *Clinical Dosimetry Measurements in Radiotherapy*, edited by D. W. O. Rogers and J. E. Cygler (Medical Physics, Madison, 2009), pp. 723–757.
[26]ICRU, "Stopping powers for electrons and positrons," ICRU Report No. 37 (ICRU, Bethesda, MD, 1984).
[27]D. W. O. Rogers and I. Kawrakow, "Monte Carlo calculated correction factors for primary standards of air-kerma," Med. Phys. **30**, 521–543 (2003).
[28]J. Wulff, J. T. Heverhagen, K. Zink, and I. Kawrakow, "Investigation of systematic uncertainties in Monte Carlo-calculated beam quality correction factors," Phys. Med. Biol. **55**, 4481–4493 (2010).
[29]L. A. Buckley, I. Kawrakow, and D. W. O. Rogers, "CSnrc: Correlated sampling Monte Carlo calculations using EGSnrc," Med. Phys. **31**, 3425–3435 (2004).
[30]I. Kawrakow, "Accurate condensed history Monte Carlo simulation of electron transport. II. Application to ion chamber response simulations," Med. Phys. **27**, 499–513 (2000).
[31]H. Svensson and A. Brahme, in *Radiation Dosimetry*, edited by C. G. Orton (Plenum, New York, 1986), pp. 87–170.